Journal of Alloys and Compounds 713 (2017) 87–94

Contents lists available at ScienceDirect

Journal of Alloys and Compounds

journal homepage: http://www.elsevier.com/locate/jalcom

Optical and microstructural properties of InGaN/GaN multiple quantum wells with embedded graphene coating

Goh-Myeong Bae [a, 1], Jae-Kyung Choi [a, e, 1], Chu-Young Cho [b], Jong-Hwa Lee [a], Jinsung Kwak [a], Hyunseok Na [c], Kyung-Ho Park [b], Kibog Park [d, **], Soon-Yong Kwon [a, *]

[a] School of Materials Science and Engineering & Low Dimensional Carbon Materials Center, Ulsan National Institute of Science and Technology (UNIST), Ulsan, 44919, South Korea
[b] Korea Advanced Nano Fab Center, Suwon, 16229, South Korea
[c] Department of Advanced Materials Science and Engineering, Daejin University, Gyeonggi, 11159, South Korea
[d] Department of Physics, Ulsan National Institute of Science and Technology (UNIST), Ulsan, 44919, South Korea
[e] SMEs Support Center, Korea Institute of Science and Technology Information (KISTI), Busan, 48058, South Korea

ARTICLE INFO

Article history:
Received 9 February 2017
Received in revised form
11 April 2017
Accepted 13 April 2017
Available online 18 April 2017

Keywords:
Nitride materials
Crystal growth
Coating materials
Nanostructured materials
Graphene

ABSTRACT

We investigate the effects of embedded graphene coating on the optical and microstructural properties of ultrathin InGaN/GaN multiple quantum wells (MQWs). The InGaN/GaN MQWs grown on graphene-buffered GaN templates displayed enhanced internal quantum efficiency compared to conventional ones and showed the internal electric field effect-free characteristic, desirable for general lighting applications. These phenomena were attributed to the enhancement of potential fluctuation with increased indium content and negligible piezoelectric polarization in ultrathin InGaN QWs, respectively. It was found that the atomically rough surface of GaN induced by embedded graphene coating efficiently relieved the biaxial compressive strain in the ultrathin InGaN/GaN QWs and enhanced the In incorporation efficiency during the InGaN growth, suggesting the potential use of atomic-thick carbon layer in niche optoelectronic applications.

1. Introduction

For the last decades, full color light sources based on III-N semiconductor light-emitting diodes (LEDs) have attracted great interest as highly energy-efficient and environmentally stable lighting technologies [1–3]. Although the development of epitaxial growth techniques such as molecular beam epitaxy and metal-organic chemical vapor deposition (MOCVD) has enabled the growth of single-crystalline III-N thin-films with excellent performance for optoelectronic device applications; however, the applications of III-N LEDs toward general lighting requires even higher brightness and efficiency [4,5]. Currently, state-of-the-art III-Ns technology has been focused on the III-N thin-film growth on a c-plane sapphire (c-sapphire) substrate using a conventional two-step growth method in a MOCVD reactor, which employs about 20-to-30-nm-thick, low-temperature (LT)-grown (Ga,Al)N buffer layers before the growth of GaN epitaxial layers at high temperatures [2,3]. It is well known that the nitride buffer growth condition has a deterministic effect on the structural and optoelectronic properties of the subsequent GaN epitaxial layers as well as active InGaN/GaN quantum wells (QWs). Generally, the heteroepitaxy of III-Ns on c-sapphire leads to strained epilayers originating from considerable differences in in-pane lattice and thermal mismatches between III-Ns and c-sapphire. This biaxial stress is responsible for the generation of high density threading dislocation or piezoelectric polarization in the subsequent InGaN/GaN QWs [6–8]. This polarization-induced, built-in piezoelectric field causes the spatial separation of electron and hole wave-functions within QWs, resulting in a red-shift of emission wavelength as well as a significant diminution of radiative recombination efficiency [8–11]. Therefore, the control of strain/stress relaxation in III-N epilayers is one of the effective approaches to obtain efficient solid-state light emitters with reduced defect density. To overcome this issue, many

* Corresponding author. School of Materials Science and Engineering & Low Dimensional Carbon Materials Center, Ulsan National Institute of Science and Technology (UNIST), Ulsan, 44919, South Korea.
** Corresponding author. Department of Physics, Ulsan National Institute of Science and Technology (UNIST), Ulsan, 44919, South Korea.
E-mail addresses: kpark@unist.ac.kr (K. Park), sykwon@unist.ac.kr (S.-Y. Kwon).
[1] Equally contributed.

http://dx.doi.org/10.1016/j.jallcom.2017.04.120
0925-8388/

approaches such as lateral epitaxial overgrowth, introduction of nanoporous or patterned substrate, and so forth were proposed [12–15]; however, those approaches resulted in process complexity as well as cost increases owing to the compulsory photolithography and subsequent complicated processes. Thus, one promising method to overcome this problem would be to develop an alternative buffer layer with a high functionality that could enable the growth of high-quality III-Ns epilayers and simplify the subsequent growth/fabrication process.

Graphene (Gr) - a two-dimensional (2D) atomic crystal of carbon - has excellent physical and chemical properties such as mechanical strength, chemical and thermal stabilities, large surface area, and is inherently impermeable to almost all atoms and molecules [16–24]. Furthermore, a single layer of graphene exhibits approximately 2.3% light absorption [25] and offers excellent electrical and thermal conductivities due to its 2D electron gas properties at room temperature (RT) [17,22,26]. These functional attributes synergistically allow Gr-based heterostructures to exhibit unique and enhanced properties and are expected them to have numerous niche applications in high-growth markets including semiconductors, photovoltaics, and LEDs in the near future [18,20–22]. In these industries, there has been increasing demand for carbon with greater stability and enhanced, uniform properties. Thus graphene can serve as a key functional coating for III-Ns. In our earlier study [18], we reported that the use of graphene as a coating layer allows one-step growth of heteroepitaxial GaN films on c-sapphire in a MOCVD reactor, simplifying the GaN growth process. To modify the surface morphology and enhance the wetting property of graphene for GaN nucleation, we employed diffusion-assisted synthesis (DAS) method to grow nanocrystalline graphene [27,28]. We found that the wetting between GaN and c-sapphire can be greatly altered by graphene coating and the overgrown GaN layer on c-sapphire becomes continuous and flat, with as little as ~0.6 nm of graphene coating. Under optimized growth condition, one-step GaN films showed highly desirable structural and optical properties, suitable for 'pseudo-substrates' in III-N LED epilayer structure [18].

In this article, we systemically investigated the effects of embedded graphene coating on the optical and microstructural properties of III-N LED epilayer structure including ultrathin InGaN/GaN multiple QWs (MQWs). The InGaN/GaN MQW structures grown on a Gr-buffered GaN template exhibited improved internal quantum efficiency (~55%) compared to conventional ones (~30%) and internal electric field effect-free characteristic from

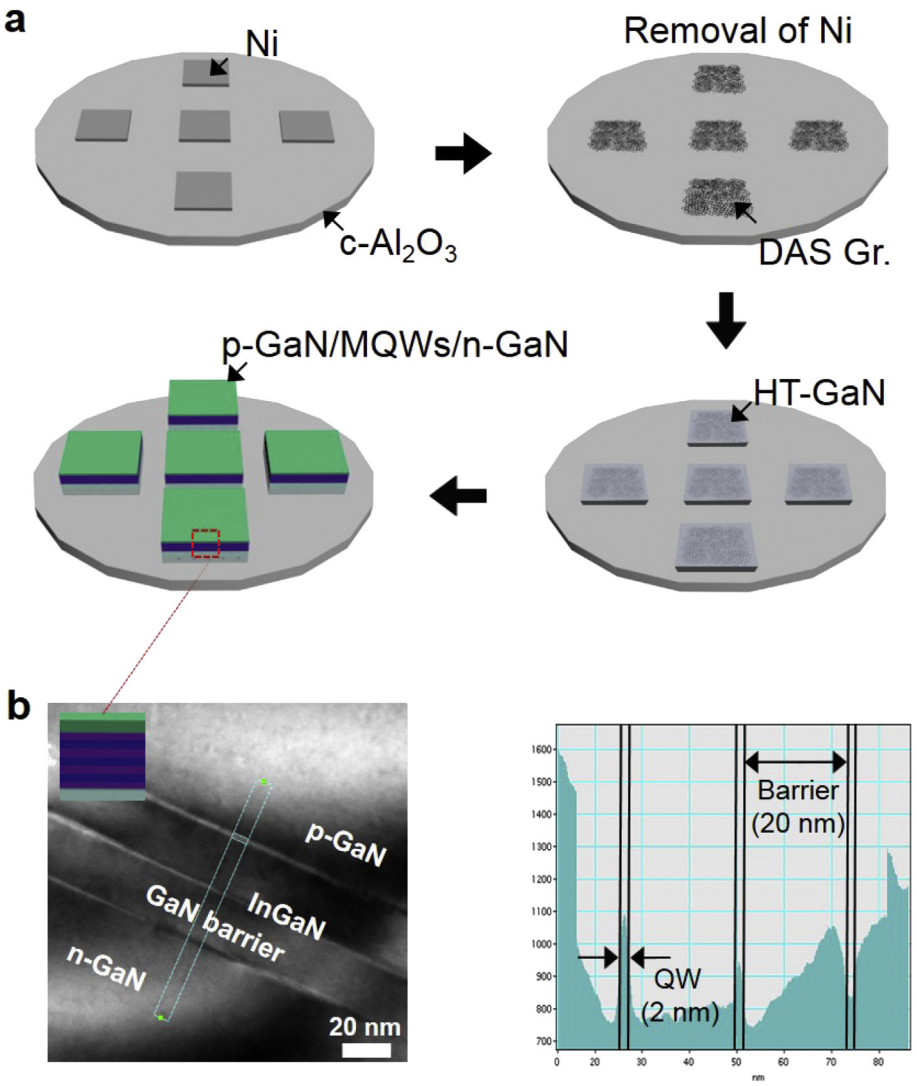

Fig. 1. (a) Scheme of patterned growth of III-N LED epilayer structure with embedded graphene coating layer, (b) Cross-sectional, bright-field HRTEM image of III-N LED epilayer structure (p-GaN/InGaN MQWs/n-GaN) and its corresponding depth profile in InGaN/GaN MQW region.

temperature- and excitation power-dependent photoluminescence (PL) studies, respectively. Monochromatic cathodoluminescence (CL) mapping and high-resolution X-ray diffraction (HRXRD) measurements implied that these phenomena were attributed to the enhancement of potential fluctuation with increased indium content and negligible piezoelectric field in an ultrathin InGaN QWs. We found that the atomically rough surface of GaN induced by graphene coating efficiently relieved the biaxial compressive strain in ultrathin InGaN/GaN QWs and enhanced the In incorporation efficiency during the InGaN growth.

2. Materials and experiment

2.1. Graphene coating on c-plane sapphire substrates

We deposited 100-nm-thick polycrystalline nickel (Ni) thin films on a double-side polished, 2-inch c-sapphire substrate at room temperature (RT) using an ultrahigh vacuum e-beam evaporator and then patterned the Ni films with a size of 10 mm × 10 mm. The average grain size of the Ni thin films deposited at RT was about 40–50 nm. We used graphite powder (Aldrich, product 496596, average diameter: ~40 μm) as a solid carbon (C) source and the patterned Ni surface was coated with graphite powder. A pressure (~1 MPa) was uniformly applied by mechanically clamping the C-Ni/sapphire diffusion couple using a 3-inch molybdenum holding stage. The assemblies were then placed in a quartz tube which is full of Ar gas and annealed at T~360 °C. Following graphene growth, the C-Ni/sapphire diffusion couples were dipped in deionized (DI) water and the Ni films were etched away using an aqueous solution of 1 M $FeCl_3$, leaving behind a nanocrystalline graphene coating layer on the c-sapphire substrate.

2.2. MOCVD growth of GaN films and III-N LED epilayer structure

After graphene coating on c-sapphire, GaN films and the subsequent InGaN/GaN MQW structures were grown in a commercial low pressure MOCVD reactor. For surface cleaning of Gr/sapphire template, a thermal annealing process was done at 1040 °C for 5 min in an N_2 atmosphere prior to GaN growth and we note that this process did not influence on the structural properties of the graphene coating layers, confirmed by optical and secondary electron microscopies (OM and SEM) [18]. The III-N epilayer structure consists of 3.5-μm-thick n-type GaN/Gr/sapphire (n-GGS) template, followed by the active region, and 70-nm-thick, p-type GaN (p-GaN) layer. The InGaN/GaN MQW active region consists of three periods of 2-nm-thick InGaN well and 20-nm-thick GaN barrier layers. The growth temperature of InGaN well, GaN barrier, and p-GaN layers was 750 °C. Trimethylgallium (TMGa), trimethylindium (TMIn), and NH_3 were used as Ga, In, and N sources, respectively. For comparison, we grew the same III-N LED epilayer structures on n-type GaN (n-GaN) films using a conventional two-step growth method and the thickness and growth temperature of LT-GaN buffer layer were about 25 nm and 500 °C, respectively.

2.3. Characterization of GaN films and III-N LED epilayer structure

The surface morphologies of the samples were observed using both an atomic force microscopy (AFM) (Veeco Multimode V) operating in tapping mode and a SEM (Hitach, S4300SE) at an acceleration voltage of 10 kV. The structural properties of the samples were examined by both high-resolution transmission electron

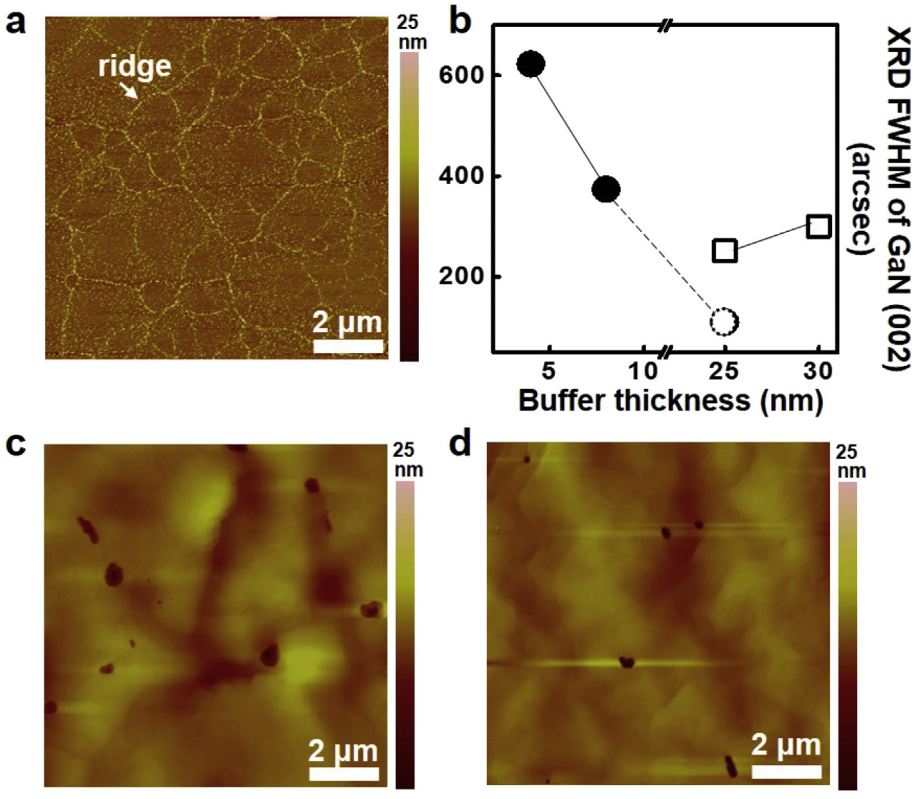

Fig. 2. (a) AFM image of a graphene film coated by the DAS process at $T = 360$ °C for 150 min on a c-sapphire substrate, (b) Plot of FWHM values in XRD ω-scan rocking curves for (0002) planes of n-GaN films grown on Gr-buffered (closed circle) and LT-GaN-buffered c-sapphire substrates (open square). The open circle is expected (c,d) AFM images of surface morphologies of (c) n-GaN film grown on a Gr-coated c-sapphire substrate and (d) p-GaN/InGaN MQWs grown on a n-GGS template.

microscopy (HRTEM) and HRXRD. The prepared TEM specimen was examined using a JEOL-JEM 3000F microscope operating at 300 kV. All the ω scan, ω-2θ scan, and reciprocal space mapping (RSM) of InGaN/GaN MQWs were obtained by an XRD (Bruker D8 Advance) using Cu Kα as the X-ray source (λ = 1.5046 Å). The optical properties of the samples were examined by PL using a He-Cd (325 nm) laser source with an output power of 30 mW and the He-Cd laser power was decreased down to 6 mW using variable ND filter for the excitation power-dependent study. Excitation power-dependent and temperature-dependent PL measurements were carried out to examine the emission mechanism in the ultrathin InGaN/GaN MQWs. For the temperature-dependent PL study, we used a cryostat, whereby the temperature of the samples was changed from RT to around 8 K while the He-Cd (325 nm) laser with a 0.2 mW output power was used as a pumping source. CL experiments were performed using a Gatan Mono CL+3 system equipped with a high-sensitivity photomultiplier tube attached to a SEM (Hitach, S-4300SE). Typical electron beam voltage was 10 kV and the current was varied from 1 pA to 1.7 nA for the beam current-dependent CL study.

3. Results and discussion

A schematic illustration of the manufacturing process is shown in Fig. 1a. Initially, nanocrystalline graphene layer was directly grown on a 2-inch c-sapphire using a DAS process [27,28] and then patterned (10 mm × 10 mm) to directly compare the growth mode of n-GaN films on c-sapphire depending on the presence of graphene coating. In our DAS process, it was found that C atoms preferentially diffuse through the grain boundaries (GBs) in a layer of Ni at low temperatures. Upon reaching the Ni/substrate interface, C atoms precipitate out as graphene at the GBs, *i.e.* graphene ridges, and growth occurs via lateral diffusion along the interface [27]. After the Ni etching process, we obtained the graphene buffer layers with high density graphene ridges for enhancing the GaN nucleation. In a MOCVD reactor, the n-GaN films were epitaxially grown on Gr-coated c-sapphire substrates. GaN crystals nucleated on the spontaneously formed, three-dimensional (3D) graphene ridge areas, and laterally overgrew 3D ridges to obtain completely coalesced, flat n-GaN thin film. The detailed microstructural properties (*e.g.* HRTEM images of the GaN/Gr interface for the ridge regions and other regions) and growth mechanism of GaN films on sapphire with graphene coating layers can be found in Ref. [18]. Without the graphene coating layer, the typical surface morphologies of n-GaN films were not always being continuous on the whole c-sapphire surface. We find that the growth behavior of the GaN films was irrelevant to the doping when the graphene coating layer was embedded. Then, we grew three periods of InGaN/GaN MQWs on the n-GGS template. From the cross-section HRTEM image, as shown in Fig. 1b, we found that the three-periods of

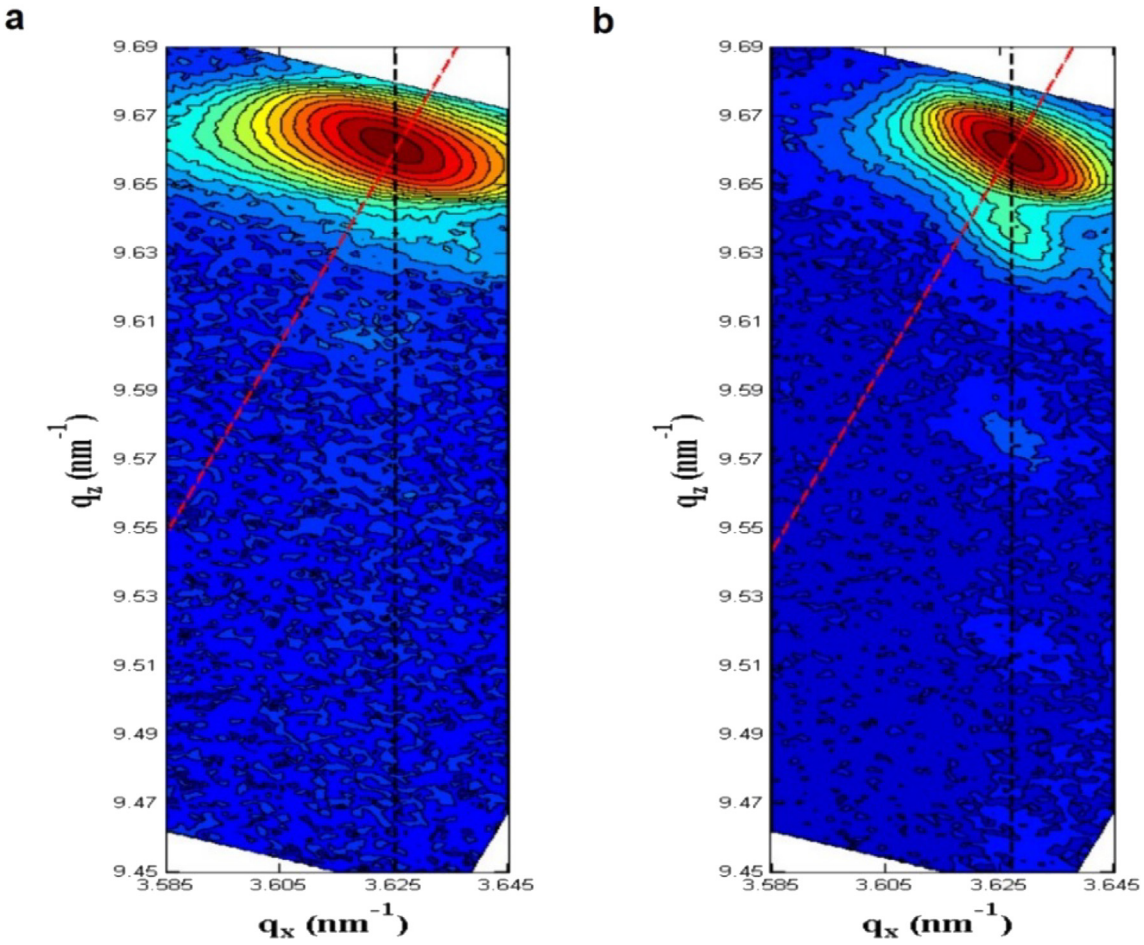

Fig. 3. Reciprocal space maps for the (105) reflections of III-N LED epilayer including (a) $In_{0.24}Ga_{0.76}N$/GaN MQWs grown on a n-GGS template and (b) $In_{0.18}Ga_{0.82}N$/GaN MQWs grown on a conventional n-TSG template. The growth conditions of the III-N LED epilayer on both GaN templates were the same in a MOCVD reactor. The black and red dashed lines indicate fully strained and fully relaxed InGaN layers in a reciprocal space, respectively. (For interpretation of the references to colour in this figure legend, the reader is referred to the web version of this article.)

InGaN(2 nm)/GaN(20 nm) MQWs with 70-nm-thick p-GaN capping layer was successfully grown on the n-GGS template and the heterosystem was of high quality.

Fig. 2a shows the typical surface morphology of graphene directly grown on a c-sapphire substrate. The as-grown layers were nanocrystalline graphene and exhibited good uniformity with neighboring spacing between graphene ridges of several tens of nanometers. For example, after the graphene coating process at $T = 360$ °C for 150 min, the thicknesses of the graphene layers and 3D graphene ridges were about 8 and 15 nm, respectively. The thickness of the graphene coating layers can be varied up to about 10 nm by changing the DAS process parameters with keeping constant the neighboring spacing between the graphene ridges [18] and we checked the crystallinity of the overgrown n-GaN films on a large scale using an HRXRD. Fig. 2b shows the full width at half maximum (FWHM) values of XRD ω-scan rocking curves for (0002) planes of n-GaN films depending on the types and thicknesses of the buffer layers. We observe that the crystallinity of the n-GGS templates was sensitive to the thickness of the graphene coating, in contrast to the conventional ones. The crystalline quality of the n-GGS template are comparable to that of conventional ones and it is noted that we have more room for improvement in the crystalline quality of GaN films in case that the thickness of graphene coating layers can be increased over 20 nm (indicated by open circle in Fig. 2b). On top of the graphene coating layer with a thickness of 8 nm, mirror-like 3.5-μm-thick n-GaN layers were obtained at $T = 1040$ °C in a MOCVD reactor. From the AFM images in Fig. 2c–d, the root-mean-square (RMS) roughnesses of n-GGS template and p-GaN/InGaN MQW/n-GGS heterosystem were measured to be about 1.56 and 1.78 nm, using 10 μm × 10 μm scan size in AFM, respectively. We note that these values were four times larger than those of conventional, two-step grown 3.5-μm-thick n-type GaN/LT-GaN/c-sapphire (n-TSG) template (~0.40 nm) and p-GaN/InGaN MQW/n-TSG heterosystem (~0.45 nm), implying that the surface roughness of n-GaN template was significantly increased at nanoscale as a result of introduction of graphene coating layer.

Fig. 3 displays the RSMs by HRXRD around (105) reflection measured from three-period InGaN/GaN MQWs grown on a n-GGS template and on a n-TSG template to detect composition and strain profiles independently [29–33]. The RSM results show that the strain relaxation process in InGaN QWs occurs only at the sample grown on a n-GGS template despite of the ultrathin thickness (~2 nm) of InGaN and the average In mole fraction (x) in $In_xGa_{1-x}N$ QW increases as the films relax. The absence of high-order satellite peaks in the sample grown on a n-GGS template implies the occurrence of solid-state intermixing of InGaN QWs with barrier GaN layers at the atomic scale [31,32]. The average In mole fractions (x) were determined to be 0.24 and 0.18 in the $In_xGa_{1-x}N$ QWs grown on a n-GGS template and on a n-TSG template, respectively. The in-plane and out-of-plane stains (ε_{xx}, ε_{zz}) as well as degree of relaxation (R) were calculated based on the equations and material constants appeared in Ref. [33]. According to the calculation, we have obtained the (ε_{xx}, ε_{zz}) = (−0.0213,−0.0099) and R = 0 (fully-strained) for $In_{0.18}Ga_{0.82}N$ grown on n-TSG template and the (ε_{xx}, ε_{zz}) = (−0.0252,−0.0199) and R = 0.07 (partially-relaxed) for $In_{0.24}Ga_{0.76}N$ grown on n-GGS template. These results clearly show that the degree of strain relaxation can influence on the amount of In that is incorporated during InGaN growth [34–39]. The In incorporation efficiency in the InGaN layer is known to be primarily complicated by the high In vapor pressure at the growth temperature and the large lattice mismatch and thermal incompatibility in the GaN-InN system. Without generation of misfit dislocations, the stresses present in an InGaN layer shift the chemical equilibrium towards enhanced desorption of In, which impairs the efficiency of In incorporation into a growing layer [37–39]. Therefore, we

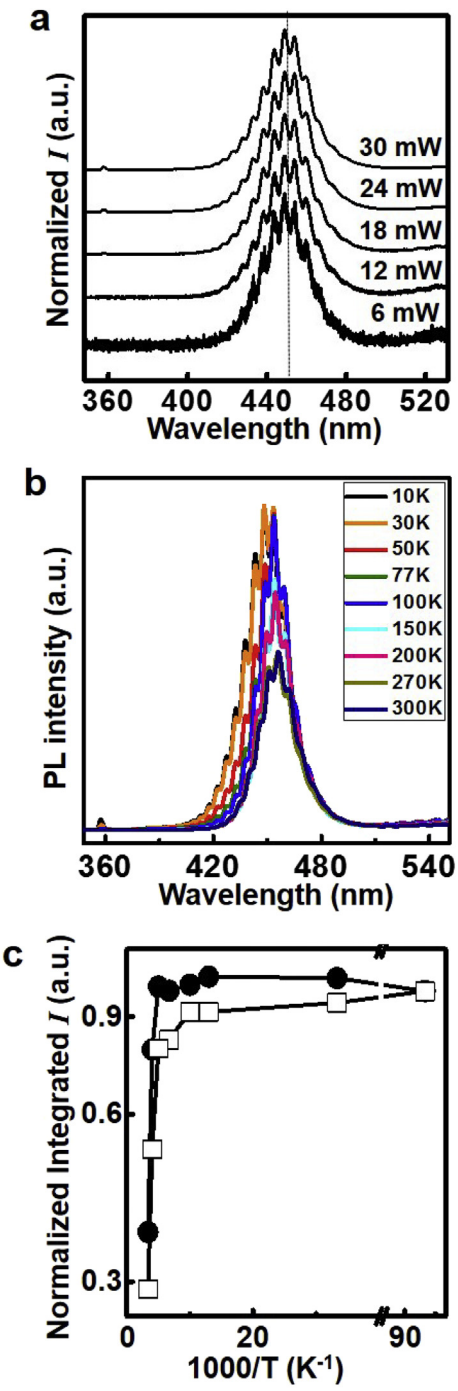

Fig. 4. (a) Excitation power-dependent RT PL spectra of three periods of InGaN/GaN MQWs grown on a n-GGS template. The excitation powers were varied from 6, 12, 18, 24–30 mW (from bottom to top). (b) Temperature-dependent PL spectra of InGaN/GaN MQWs grown on a n-GGS template measured at 10, 30, 50, 77, 100, 150, 200, 270, and 300 K. (c) Normalized integrated PL intensity as a function of 1/T for InGaN/GaN MQWs grown on a n-GGS template (closed circle) and on a conventional n-TSG template (open square).

suggest that the atomically rough GaN surface morphology in a n-GGS template plays a critical role in spontaneously relieving the biaxial compressive strain in the ultrathin InGaN QWs, thereby enhancing the In incorporation efficiency during InGaN growth.

To investigate optical properties, PL measurements were carried out on the InGaN/GaN MQW samples. The RT PL spectra from the InGaN/GaN MQWs grown on a n-GGS template and on a n-TSG

template showed a strong blue emission at around 462 and 447 nm, respectively. The PL peak position at 462 nm is red-shifted by about 0.09 eV compared to that of 447 nm, which corresponds to the increased In mole fraction of InGaN QWs grown on a n-GGS template compared to that on a n-TSG template. To further explore the emission mechanism, we performed excitation power- and temperature-dependent PL measurements. From excitation power-dependent PL, the intensities of blue emission peaks markedly increased and showed no saturation behavior in both samples, proving that the blue emission peaks were from the InGaN QWs, and not from any defect levels. Fig. 4a shows that, with increasing excitation power from 6 to 30 mW, the PL energies of the QW peak remained nearly unchanged in a sample grown on a n-GGS template. This indicates that the piezoelectric effect, frequently observed in conventional InGaN MQWs [4,13], was sufficiently suppressed in the InGaN MQWs grown on a n-GGS template, which would be desirable for general lighting applications. It is clear that internal electric field effect weakened with decrease of InGaN well width [2,3]. Although the internal electric field in the InGaN MQW grown on a n-GGS template would be quite weak due to the ultrathin (2 nm) well width, a significant blue shift of around 10 nm in PL peak is expected from calculation of eight band $k \cdot p$ method, as observed in the InGaN MQW grown on a n-TSG template. However, we cannot observe any peak shift with increasing excitation power in the InGaN MQWs grown on a n-GGS template. This phenomenon can be attributed to the relieved compressive strain in InGaN MQWs grown on a rough n-GGS template and/or the high residual carrier density over 10^{18} cm^{-3} in the InGaN well, which is enough density to screen the internal electric field [11,40–42].

Fig. 4b shows temperature-dependent PL spectra acquired from 8 to 300 K for the ultrathin InGaN/GaN MQWs grown on a n-GGS template. The emission peaks from the InGaN QWs are clearly seen

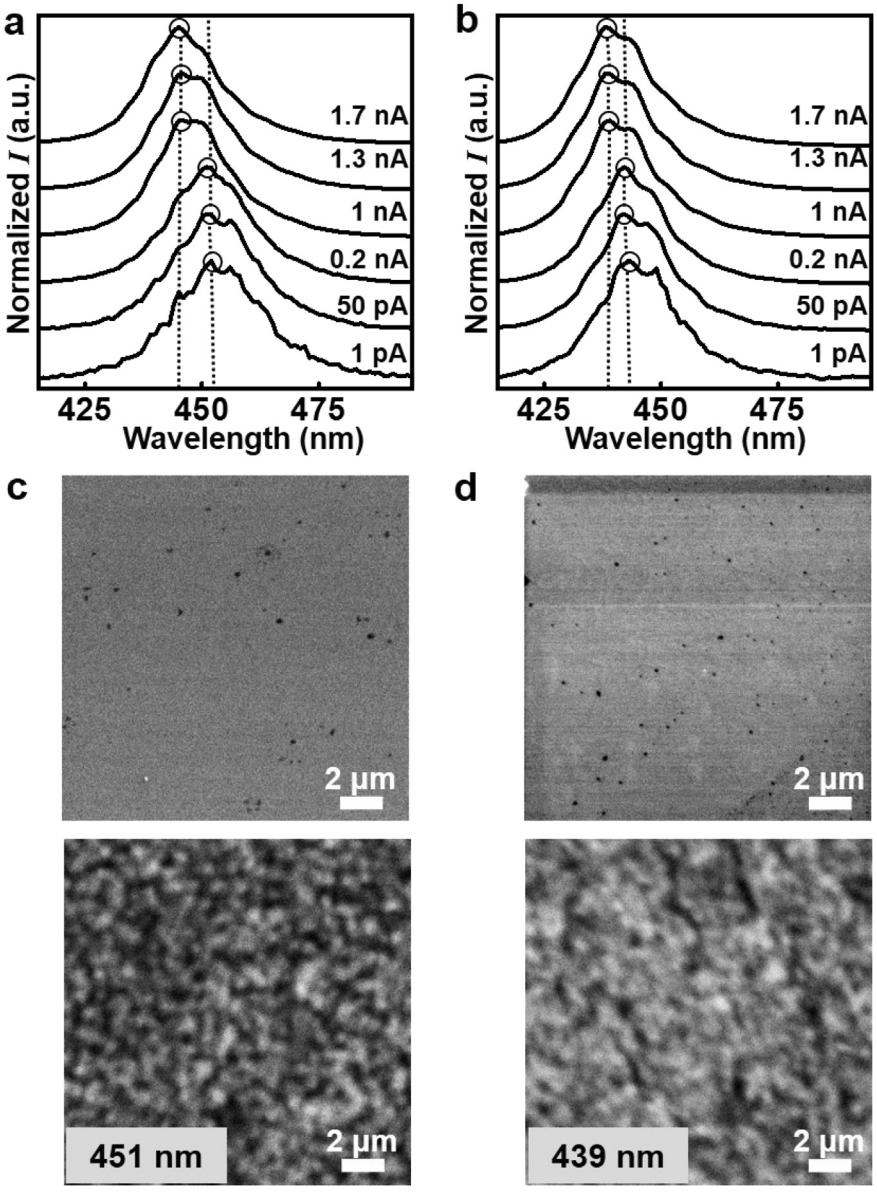

Fig. 5. (a,b) Normalized CL spectra of the III-N LED epilayer structures grown (a) on a n-GGS template and (b) on a conventional n-TSG template and. The beam currents were varied from 1 pA, 50 pA, 200 pA, 1 nA, 1.3 nA, to 1.7 nA (from bottom to top). (c,d) (top) SEM images and (bottom) corresponding spatially resolved monochromatic 77 K CL mapping images of III-N LED epilayer structures (p-GaN/InGaN MQWs/n-GaN) grown (c) on a n-GGS template and (d) on a conventional n-TSG template. The CL mapping images in (c) and (d) were taken at 451 nm and 439 nm, respectively.

from the sample and, as measuring temperature increased to RT, the emission intensity of the QW peak decreased by less than one order of magnitude, compared to that measured at 8 K, as shown in Fig. 4c. We defined the internal quantum efficiency η_{PL} as the ratio of the integrated PL intensities between measuring temperature T and 8 K, as $\eta_{PL} = I_T/I_{8K}$, and the value (η_{PL}) was calculated as around 0.55 at an excitation intensity level of around ~15 kW cm^{-2}. For comparison, the value (η_{PL}) of the same MQW structure grown on a n-TSG template was measured to be around 0.3. Improved thermal stability in the emission process from the sample grown on a n-GGS template suggests the formation of carrier localization centers in the ultrathin InGaN MQWs. It has been reported that the high luminescence efficiency in InGaN QWs results from self-formed In-rich regions in spite of the large defect density in InGaN layers [43–46].

To study the presence and nature of localized states in two-types of InGaN MQWs grown on different GaN templates, current-dependent CL spectra measurements and spatially resolved monochromatic CL mapping were carried out at 77 K. The CL spectra from the MQWs grown on a n-GGS template and on a n-TSG template show a clear blue emission at around 451 and 439 nm, respectively, as shown in Fig. 5a–b. Interestingly, the InGaN MQWs grown on a n-GGS template exhibited a significant blue-shift of around 43 meV compared to the MQWs grown on a n-TSG template (around 23 meV) when e-beam current was varied from 1.0 pA to 1.7 nA, suggesting the presence of a deep potential well in the InGaN QWs grown on a n-GGS template. It is well known that the potential fluctuation in InGaN QWs can be induced by In compositional fluctuations, interface roughness, as well as structural defects [4]. For the MQW grown on a n-GGS template (Fig. 5c), the CL mapping image clearly displays that small cluster structures cover the full fields and all the emissions are from the 3D quantum dot (QD)-like In-rich InGaN cluster structures. In addition, the sample showed increased interfacial and surface roughnesses from the RSM and AFM measurements, respectively. For the MQWs grown on a n-TSG template (Fig. 5d), because the GaN surface is atomically smooth and flat, the clusters have joined together to form a relatively smooth surface that give 2D QW-like environment in its energy band structure. From the results, it is imperative that the InGaN MQWs grown on a n-GGS template shows the improved thermal stability than that grown on a TSG template, resulting in high internal quantum efficiency as observed in Fig. 4c. For comparison, we grew the $In_xGa_{1-x}N$ MQWs with $x = 0.25$ on a n-TSG template and observed the formation of 3D QD-like In-rich InGaN cluster structures in the CL mapping image, implying that the QD formation is primarily due to the increased In composition in the MQWs although the increased interfacial and surface roughnesses may affect on the formation of InGaN QDs. The enhanced potential fluctuation in QWs would cause carriers to be localized in potential minima, thus preventing carriers from reaching nonradiative defects such as dislocations. This explains why the emission intensity of the MQWs grown on a n-GGS template less sensitively decreases with increasing temperature than the MQWs grown on a n-TSG template.

4. Conclusions

The III-N LED epilayer structures were grown by MOCVD on different types of GaN templates. Optical properties were systemically investigated by excitation power-dependent and temperature-dependent PL and CL techniques. Higher quantum efficiency of the emission with electric field effect-free property was found for the sample grown on Gr-buffered GaN template than conventional one. Both PL and CL observations showed that 3D QD-like cluster structures are formed for the InGaN QWs grown on Gr-buffered GaN templates, while the InGaN QWs grown on conventional one forms a relatively 2D QW-like environment in its energy band structure. We found that the embedded graphene coating efficiently relieved the biaxial compressive strain in the ultrathin InGaN/GaN QWs by the surface roughness of the underlying GaN surface, thus forming 3D QD-like clusters in the QWs.

Acknowledgements

This work was supported by the National Research Foundation (NRF) funded by the Korean government through the Bio and Medical Technology Development Program (Grant No. NRF-2012M3A9C6049797), the Midcareer Researcher Program (Grant No. NRF-2013R1A2A2A04015946), and through the Basic Science Research Program (Grant No. NRF-2016R1A2B4014762).

References

[1] S. Pimputkar, J.S. Speck, S.P. DenBaars, S. Nakamura, Prospects for LED lighting, Nat. Photonics 3 (2009) 179–181.
[2] I. Akasaki, Blue light: a fascinating journey, Angew. Chem. Int. Ed. 54 (2015) 7750–7763.
[3] E.F. Schubert, Light-emitting Diodes, second ed., Cambridge University Press, 2006.
[4] M.R. Krames, O.B. Shchekin, R. Mueller-Mach, G.O. Mueller, L. Zhou, G. Harbers, M.G. Craford, Status and future of high-power light-emitting diodes for solid-state lighting, J. Disp. Technol. 3 (2007) 160–175.
[5] Z. Zang, X. Zeng, J. Du, M. Wang, X. Tang, Femtosecond laser direct writing of microholes on roughened ZnO for output power enhancement of InGaN light-emitting diodes, Opt. Lett. 41 (2016) 3463–3466.
[6] T. Hashimoto, F. Wu, J.S. Speck, S. Nakamura, A GaN bulk crystal with improved structural quality grown by the ammonothermal method, Nat. Mater. 6 (2007) 568–571.
[7] J. Kim, H. Woo, K. Joo, S. Tae, J. Park, D. Moon, S.H. Park, J. Jang, Y. Cho, J. Park, H. Yuh, G.D. Lee, I.S. Choi, Y. Nanishi, H.N. Han, K. Char, E. Yoon, Less strained and more efficient GaN light-emitting diodes with embedded silica hollow nanospheres, Sci. Rep. 3 (2013) 3201.
[8] H. Amano, Growth of GaN layers on sapphire by low-temperature-deposited buffer layers and realization of p-type GaN by magnesium doping and electron beam irradiation, Angew. Chem. Int. Ed. 54 (2015) 7764–7769.
[9] M.F. Schubert, S. Chhajed, J.K. Kim, E.F. Schubert, D.D. Koleske, M.H. Crawford, S.R. Lee, A.J. Fischer, G. Thaler, M.A. Banas, Effect of dislocation density on efficiency droop in GaInN/GaN light-emitting diodes, Appl. Phys. Lett. 91 (2007) 231114.
[10] S.-Y. Kwon, H.J. Kim, E. Yoon, Y.D. Jang, K.J. Yee, D.H. Lee, S.H. Park, D.Y. Park, H. Cheong, F. Rol, L.S. Dang, Optical and microstructural studies of atomically flat ultrathin In-rich InGaN/GaN multiple quantum wells, J. Appl. Phys. 103 (2008) 063509.
[11] A. Armstrong, T.A. Henry, D.D. Koleske, M.H. Crawford, K.R. Westlake, S.R. Lee, Dependence of radiative efficiency and deep level defect incorporation on threading dislocation density for InGaN/GaN light emitting diodes, Appl. Phys. Lett. 101 (2012) 162102.
[12] O.H. Nam, M.D. Bremser, T.S. Zheleva, R.F. Davis, Lateral epitaxy of low defect density GaN layers via organometallic vapor phase epitaxy, Appl. Phys. Lett. 71 (1997) 2638–2640.
[13] P. Frajtag, N.A. El-Masry, N. Nepal, S.M. Bedair, Embedded voids approach for low defect density in epitaxial GaN films, Appl. Phys. Lett. 98 (2011) 023115.
[14] B.-R. Yeom, R. Navamathavan, J.-H. Park, Y.-H. Ra, C.-R. Lee, Growth behavior of GaN epilayers on Si(111) grown by GaN nanowires assisted epitaxial lateral overgrowth, CrystEngComm 14 (2012) 5558–5563.
[15] D.W. Jeon, H.S. Cho, J.W. Park, L.W. Jang, M. Kim, J.W. Jeon, J.W. Ju, J.H. Baek, I.-H. Lee, Separation of laterally overgrown GaN template by using selective electrochemical etching, J. Alloy. Compd. 542 (2012) 59–62.
[16] K.S. Novoselov, A.K. Geim, S.V. Morozov, D. Jiang, Y. Zhang, S.V. Dubonos, I.V. Grigorieva, A.A. Firsov, Electric field effect in atomically thin carbon films, Science 306 (2004) 666–669.
[17] A.A. Balandin, S. Ghosh, W.Z. Bao, I. Calizo, D. Teweldebrhan, F. Miao, C.N. Lau, Superior thermal conductivity of single-layer graphene, Nano Lett. 8 (2008) 902–907.
[18] J.-K. Choi, J.H. Huh, S.D. Kim, D. Moon, D. Yoon, K. Joo, J. Kwak, J.H. Chu, S.Y. Kim, K. Park, Y.W. Kim, E. Yoon, H. Cheong, S.-Y. Kwon, One-step graphene coating of heteroepitaxial GaN films, Nanotechnology 23 (2012) 435603.
[19] D. Akinwande, N. Petrone, J. Hone, Two-dimensional flexible nanoelectronics, Nat. Commun. 5 (2014) 5678.
[20] X.M. Wang, H. Tian, M.A. Mohammad, C. Li, C. Wu, Y. Yang, T.L. Ren, A spectrally tunable all-graphene-based flexible field-effect light-emitting device, Nat. Commun. 6 (2015) 7767.
[21] Y.D. Liu, F.Q. Wang, X.M. Wang, X.Z. Wang, E. Flahaut, X.L. Liu, Y. Li, X.R. Wang, Y.B. Xu, Y. Shi, R. Zhang, Planar carbon nanotube-graphene hybrid films for

high-performance broadband photodetectors, Nat. Commun. 6 (2015) 8589.
[22] J.H. Chu, D.H. Lee, J. Jo, S.Y. Kim, J.-W. Yoo, S.-Y. Kwon, Highly conductive and environmentally stable organic transparent electrodes laminated with graphene, Adv. Funct. Mater. 26 (2016) 7234–7243.
[23] H. Han, Y. Zhang, N. Wang, M.K. Samani, Y. Ni, Z.Y. Mijbil, M. Edwards, S. Xiong, K. Saaskilahti, M. Murugesan, Y. Fu, L. Ye, H. Sadeghi, S. Bailey, Y.A. Kosevich, C.J. Lambert, J. Liu, S. Volz, Functionalization mediates heat transport in graphene nanoflakes, Nat. Commun. 7 (2016) 11281.
[24] S.-Y. Kim, J. Kwak, J.H. Kim, J.-U. Lee, Y. Jo, S.Y. Kim, H. Cheong, Z. Lee, S.-Y. Kwon, Substantial improvements of long-term stability in encapsulation-free WS_2 using highly interacting graphene substrate, 2D Mater. 4 (2017) 011007.
[25] R.R. Nair, P. Blake, A.N. Grigorenko, K.S. Novoselov, T.J. Booth, T. Stauber, N.M.R. Peres, A.K. Geim, Fine structure constant defines visual transparency of graphene, Science 320 (2008), 1308–1308.
[26] K.I. Bolotin, K.J. Sikes, Z. Jiang, M. Klima, G. Fudenberg, J. Hone, P. Kim, H.L. Stormer, Ultrahigh electron mobility in suspended graphene, Solid State Commun. 146 (2008) 351–355.
[27] J. Kwak, J.H. Chu, J.-K. Choi, S.-D. Park, H. Go, S.Y. Kim, K. Park, S.D. Kim, Y.-W. Kim, E. Yoon, S. Kodambaka, S.-Y. Kwon, Near room-temperature synthesis of transfer-free graphene films, Nat. Commun. 3 (2012) 645.
[28] J.H. Chu, J. Kwak, S.D. Kim, M.J. Lee, J.J. Kim, S.D. Park, J.-K. Choi, G.H. Ryu, K. Park, S.Y. Kim, J.H. Kim, Z. Lee, Y.-W. Kim, S.-Y. Kwon, Monolithic graphene oxide sheets with controllable composition, Nat. Commun. 5 (2014) 3383.
[29] S. Pereira, M.R. Correia, E. Pereira, K.P. O'Donnell, E. Alves, A.D. Sequeira, N. Franco, I.M. Watson, C.J. Deatcher, Strain and composition distributions in wurtzite InGaN/GaN layers extracted from x-ray reciprocal space mapping, Appl. Phys. Lett. 80 (2002) 3913–3915.
[30] C.J. Neufeld, N.G. Toledo, S.C. Cruz, M. Iza, S.P. DenBaars, U.K. Mishra, High quantum efficiency InGaN/GaN solar cells with 2.95 eV band gap, Appl. Phys. Lett. 93 (2008) 3913.
[31] S.-Y. Kwon, H.J. Kim, H. Na, Y.W. Kim, H.C. Seo, H.J. Kim, Y. Shin, E. Yoon, Y.S. Park, In-rich InGaN/GaN quantum wells grown by metal-organic chemical vapor deposition, J. Appl. Phys. 99 (2006) 044906.
[32] M.A. Sousa, T.C. Esteves, N.B. Sedrine, J. Rodrigues, M.B. Lourenco, A. Redondo-Cubero, E. Alves, K.P. O'Donnell, M. Bockowski, C. Wetzel, M.R. Correia, K. Lorenz, T. Monteiro, Luminescence studies on green emitting InGaN/GaN MQWs implanted with nitrogen, Sci. Rep. 5 (2015) 9703.
[33] J.J. Xue, D.J. Chen, B. Liu, H. Lu, R. Zhang, Y.D. Zheng, B. Cui, A.M. Wowchak, A.M. Dabiran, K. Xu, J.P. Zhang, Indium-rich InGaN epitaxial layers grown pseudomorphically on a nano-sculpted InGaN template, Opt. Express 20 (2012) 8093–8099.
[34] K. Hiramatsu, Y. Kawaguchi, M. Shimizu, N. Sawaki, T. Zheleva, R.F. Davis, H. Tsuda, W. Taki, N. Kuwano, K. Oki, The composition pulling effect in MOVPE grown InGaN on GaN and AlGaN and its TEM characterization, MRS Internet, J. N. S. R. 2 (1997) 6.
[35] I.K. Park, M.K. Kwon, S.H. Baek, Y.W. Ok, T.Y. Seong, S.J. Park, Y.S. Kim, Y.T. Moon, D.J. Kim, Enhancement of phase separation in the InGaN layer for self-assembled In-rich quantum dots, Appl. Phys. Lett. 87 (2005) 061906.
[36] L.W. Jang, D.W. Jeon, A.Y. Polyakov, A.V. Govorkov, V.N. Sokolov, N.B. Smirnov, H.S. Cho, J.H. Yun, K.D. Shcherbatchev, J.H. Baek, I.-H. Lee, Electrical and structural properties of GaN films and GaN/InGaN light-emitting diodes grown on porous GaN templates fabricated by combined electrochemical and photoelectrochemical etching, J. Alloy. Compd. 589 (2014) 507–512.
[37] C.B. Soh, S.Y. Chow, L.Y. Tan, H. Hartono, W. Liu, S.J. Chua, Enhanced luminescence efficiency due to carrier localization in InGaN/GaN heterostructures grown on nanoporous GaN templates, Appl. Phys. Lett. 93 (2008) 173107.
[38] A.V. Sakharov, W.V. Lundin, E.E. Zavarin, M.A. Sinitsyn, A.E. Nikolaev, S.O. Usov, V.S. Sizov, G.A. Mikhailovsky, N.A. Cherkashin, M. Hytch, F. Hue, E.V. Yakovlev, A.V. Lobanova, A.F. Tsatsulnikov, Effect of strain relaxation on active-region formation in InGaN/(Al)GaN heterostructures for green LEDs, Semiconductors 43 (2009) 812–817.
[39] A.H. Park, T.H. Seo, S. Chandramohan, G.H. Lee, K.H. Min, S. Lee, M.J. Kim, Y.G. Hwang, E.-K. Suh, Efficient stress-relaxation in InGaN/GaN light-emitting diodes using carbon nanotubes, Nanoscale 7 (2015) 15099.
[40] S.-Y. Kwon, M.-H. Cho, P. Moon, H.J. Kim, H. Na, H.-C. Seo, H.J. Kim, Y. Shin, D.W. Moon, Y. Sun, Y.-H. Cho, E. Yoon, Near-UV emission from In-rich InGaN/GaN single quantum well structure with compositional grading, Phys. Stat. Sol. A 201 (2004) 2818–2822.
[41] S. Schulz, E.P. O'Reilly, Theory of reduced built-in polarization field in nitride-based quantum dots, Phys. Rev. B 82 (2010) 033411.
[42] S. De, A. Layek, S. Bhattacharya, D.K. Das, A. Kadir, A. Bhattacharya, S. Dhar, A. Chowdhury, Quantum-confined stark effect in localized luminescent centers within InGaN/GaN quantum-well based light emitting diodes, Appl. Phys. Lett. 101 (2012) 121919.
[43] C.H. Lu, Y.C. Li, Y.H. Chen, S.C. Tsai, Y.L. Lai, Y.L. Li, C.-P. Liu, Output power enhancement of InGaN/GaN based green light-emitting diodes with high-density ultra-small In-rich quantum dots, J. Alloy. Compd. 555 (2013) 250–254.
[44] J.H. Kim, Y.H. Ko, J.H. Cho, S.H. Gong, S.M. Ko, Y.H. Cho, Toward highly radiative white light emitting nanostructures: a new approach to dislocation-eliminated GaN/InGaN core-shell nanostructures with a negligible polarization field, Nanoscale 6 (2014) 14213–14220.
[45] W. Liu, D.G. Zhao, D.S. Jiang, P. Chen, Z.S. Liu, J.J. Zhu, M. Shi, D.M. Zhao, X. Li, J.P. Liu, S.M. Zhang, H. Wang, H. Yang, Localization effect in green light emitting InGaN/GaN multiple quantum wells with varying well thickness, J. Alloy. Compd. 625 (2015) 266–270.
[46] S.-C. Tsai, H.-C. Fang, Y.-L. Lai, C.-H. Lu, C.-P. Liu, Efficiency enhancement of green light emitting diodes by improving the uniformity of embedded quantum dots in multiple quantum wells through working pressure control, J. Alloy. Compd. 669 (2016) 156–160.